Ore Geology Reviews 78 (2016) 346–360

Contents lists available at ScienceDirect

Ore Geology Reviews

journal homepage: www.elsevier.com/locate/oregeorev

Geological, geochronological, and H–O isotopic constraints on the genesis of the Tongjing Cu–Au deposit in the Ningwu basin, east China

Jin-Jie Yu [a,*], Tie-Zhu Wang [a], Lin-Rui Che [b], Bang-Cheng Lu [c]

[a] MLR Key Laboratory of Metallogeny and Mineral Assessment, Institute of Mineral Resources, Chinese Academy of Geological Sciences, Beijing 100037, China
[b] Sino-mine Resource Exploration Co., Limited, Beijing 100089, China
[c] Faculty of Geosciences, China University of Geosciences, Beijing 100083, China

ARTICLE INFO

Article history:
Received 14 December 2015
Received in revised form 7 April 2016
Accepted 11 April 2016
Available online 23 April 2016

Keywords:
Ore-forming stage
Hydrogen and oxygen isotopes
LA–MC–ICP–MS zircon U–Pb dating
^{40}Ar–^{39}Ar age of sericite
Genetic model
Tongjing Cu–Au deposit
Ningwu basin

ABSTRACT

The Tongjing Cu–Au deposit is a medium-sized deposit within the Ningwu volcanic basin, east China, and is hosted by Cretaceous volcanic rocks of the Dawangshan and Niangniangshan Formations. The veined and lenticular Cu–Au orebodies are spatially and temporally related to the volcanic and subvolcanic rocks of the Niangniangshan Formation in the ore district. The wall-rock alteration is dominated by silicification, siderite alteration, carbonation, sericitization, chloritization, and kaolinization. On the basis of field evidence and petrographic observations, two stages of mineralization are recognized: (1) a siderite–quartz–sulfide stage (Stage 1) associated with the formation of chalcopyrite and pyrite in a quartz and siderite gangue; and (2) a quartz–bornite stage (Stage 2) cutting the Stage 1 phases. Stage 1 is the main mineralization stage. Quartz that formed in Stage 1 has $\delta^{18}O_{H2O}$ values of −4.3‰ to 3.5‰ with δD values of fluid inclusion waters of −97.1‰ to −49.9‰, indicating that the ore-forming fluids were derived from early magmatic fluids and may have experienced oxygen isotopic exchange with meteoric water during Stage 1 mineralization.

LA–MC–ICP–MS zircon U–Pb dating of the mineralization-related nosean-bearing phonolite and nosean-bearing phonolitic brecciated tuff at Tongjing yields ages of 129.8 ± 0.5 Ma and 128.9 ± 1.1 Ma, respectively. These results are interpreted as the crystallization age of the volcanic rocks of the Niangniangshan Formation. A hydrothermal sericite sample associated with Cu–Au mineralization at Tongjing yields a plateau ^{40}Ar–^{39}Ar age of 131.3 ± 1.3 Ma. These results confirm a genetic link between the volcanism and associated Cu–Au mineralization. The Tongjing Cu–Au deposit in the Ningwu basin is genetically and possibly tectonically similar to alkaline intrusion-related gold deposits elsewhere in the world.

1. Introduction

The Tongjing Cu–Au deposit is located in the central part of the Ningwu (Nanjing–Wuhu) volcanic basin of the Middle and Lower Yangtze River Valley (MLYRV) metallogenic belt (Fig. 1). This belt is an important Cu–Fe–Au–S mining district in China that includes >200 ore deposits associated with Mesozoic magmatism (Chang et al., 1991; Zhai et al., 1992; Pan and Dong, 1999; Zhou et al., 2013). The Ningwu volcanic basin in east China hosts Fe-oxide–apatite, Cu–Au, and pyrite ore deposits (Yu et al., 2015b). Previous studies of the Fe-oxide–apatite deposits were mainly focused on the geology, alteration zoning, and geochemistry of these deposits (Ningwu Research Group, 1978; Zhang, 1979; Chen et al., 1981; Li and Xie, 1984; Institute of Geochemistry, Chinese Academy of Sciences, 1987; Lu et al., 1990; Xu, 1990; Chang et al., 1991; Zhai et al., 1992; Tang et al., 1998; Lin, 1999; Hou et al., 2009b, 2010, 2011, 2012; Mao et al., 2012), in an attempt to constrain the type, origin, and source of ore-forming fluids in this area. These Fe-oxide–apatite deposits, which are designated as porphyry iron deposits in the Chinese literature (Ningwu Research Group, 1978), are temporally, spatially, and genetically associated with subvolcanic plutons consisting of gabbro–diorite porphyry and/or pyroxene diorite. Hou et al. (2009b, 2010, 2011, 2012) also described the geology of the Gushan and Washan deposits, and, based on the geochemistry of mineralization-associated subvolcanic plutons, proposed an iron-oxide melt model for the origin of the Gushan and Washan deposits. Recent zircon U–Pb analyses of volcanic rocks from the Ningwu basin yielded ages of 135–127 Ma, clustering around 130 Ma (Zhang et al., 2003; Yan et al., 2009a; Zhou et al., 2011). $^{40}Ar/^{39}Ar$ dating of phlogopite associated with the Fe-oxide–apatite deposits in the Ningwu basin yielded ages of 135–127 Ma (Yu and Mao, 2004; Yuan et al., 2010; Zhou et al., 2013), consistent with the zircon U–Pb ages (132–123 Ma, Hu and Jiang, 2010; Hou and Yuan, 2010; Xue et al., 2010; Duan et al., 2011; Hou et al., 2012; Zhou et al., 2013) of the associated subvolcanic plutons. The volcanic and subvolcanic plutons in the Ningwu basin are shoshonitic, and were generally sourced from an enriched mantle that was metasomatized by interaction with subducted oceanic sediment (Wang et al., 1996, 2001, 2006). These shoshonitic rocks formed in an

* Corresponding author.
E-mail address: yjjchina@sina.com (J.-J. Yu).

http://dx.doi.org/10.1016/j.oregeorev.2016.04.005
0169-1368/

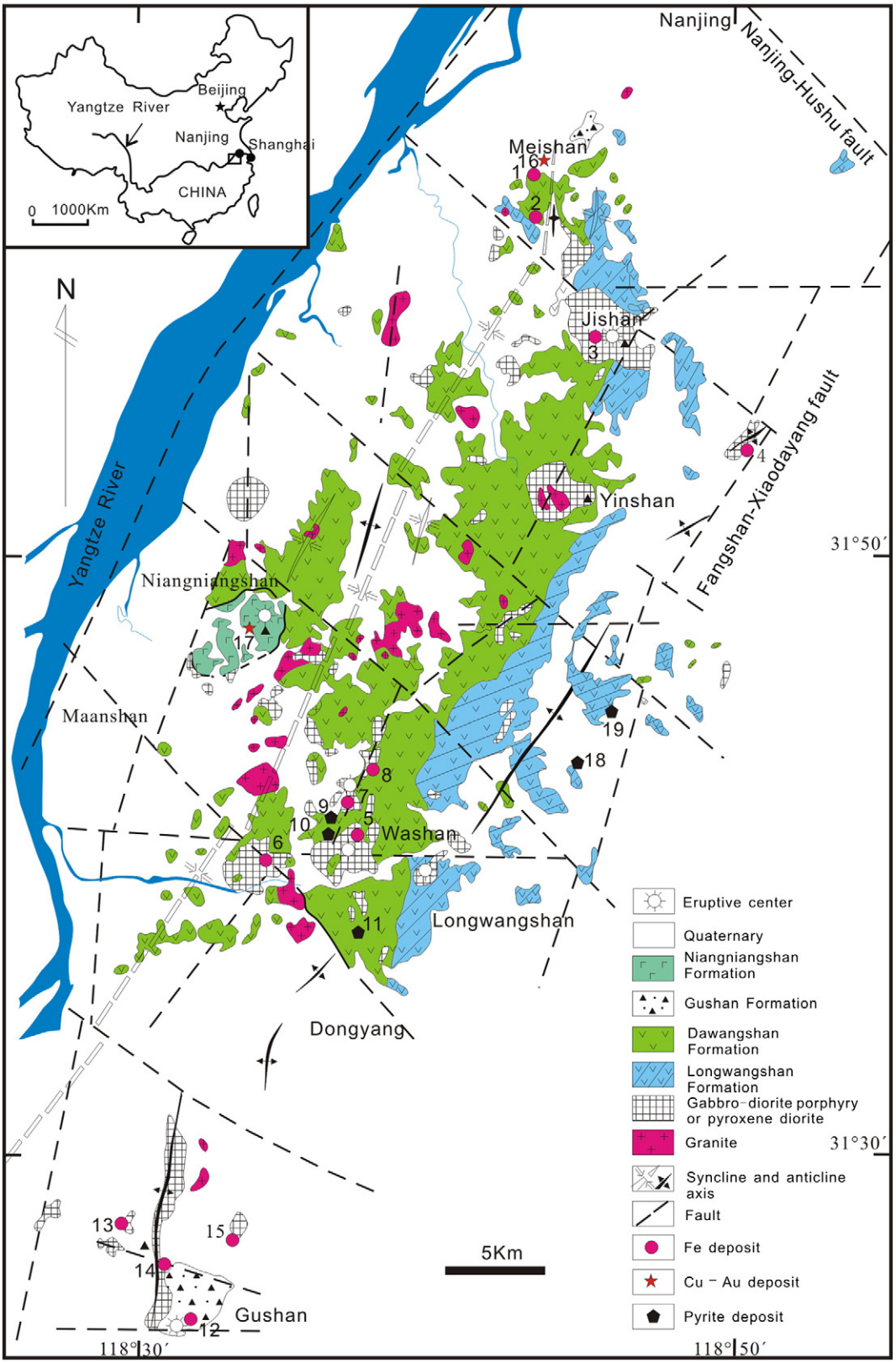

Fig. 1. Geology of the Ningwu basin (modified from Ningwu Research Group, 1978), showing the location of the Tongjing copper–gold deposit, as well as other important deposits in the region: 1 = Meishan (Fe); 2 = Taishan; 3 = Jishan; 4 = Fenghuangshan; 5 = Washan; 6 = Heshangqiao; 7 = Nanshan; 8 = Taocun; 9 = Xiangshan; 10 = Xiangshannan; 11 = Mashan; 12 = Gushan;13 = Hemushan; 14 = Zhongjiu; 15 = Baixiangshan; 16 = Meishan (Cu–Au); 17 = Tongjing; 18 = Tiantaishan; 19 = Yuntaishan.

intra-continental extensional setting where partial melting of enriched mantle material was probably controlled by lithospheric thinning and upwelling of hot asthenosphere in eastern China, which resulted from subduction of the Kula–Pacific Plate (Wu et al., 2005; Mao et al., 2006, 2011, 2012; Wang et al., 2006; Zhou et al., 2013). In addition, Yu et al. (2011) suggested that the Fe-oxide–apatite deposits of the Ningwu

basin are genetically similar and may have formed in a tectonic environment identical to that of the Kiruna-type deposits in northern Sweden. However, the majority of the previous research has been undertaken on Fe-oxide–apatite deposits in the Ningwu basin, and little attention was focused on the Cu–Au deposits of this area. In a study the alteration, oxygen isotopes, and fluid inclusions of the Meishan Fe-oxide–apatite deposit within the Ningwu volcanic basin, Yu et al. (2015a) suggested that the magnetite–apatite ore and gold ore of the Meishan deposit formed in a large-scale magmatic–hydrothermal system.

The Tongjing Cu–Au deposit has been intermittently explored by the Bureau of Geology and Minerals Resources and the Metallurgical Geological Exploration Company of Jiangsu Province since the 1950s, and contains an estimated 13 t of Au metal at an average grade of 3.5 g/t (Jiangsu Geological Survey, 2010). Exploration in this ore district continues. Gao et al. (2015) described the geological characteristics of the Tongjing Cu–Au deposit. Yu et al. (2015b) reported sulfur isotopic compositions for the sulfides within the Tongjing Cu–Au deposit, and proposed the derivation of sulfur from a single source, most probably magmatic. The quartz–siderite–sulfide veins associated with Cu–Au mineralization in the Tongjing deposit contain fluid inclusions with moderate homogenization temperatures (210–270 °C) and moderate to low salinities (12–22 wt.% NaCl equiv.; Yu et al., 2015b). However, little attention was focused on the Tongjing Cu–Au deposit. Apart from the studies of Yu et al. (2015b) and Gao et al. (2015), no geological, geochronological, and H–O isotopic data are available for the Tongjing deposit. Therefore, the origin of this deposit remains unclear.

Here we describe the geology of the Tongjing Cu–Au deposit, and report zircon U–Pb ages for nosean-bearing phonolite and nosean-bearing phonolitic brecciated tuff that are spatially linked with the Cu–Au mineralization. We also report an Ar–Ar age for sericite that is associated with the Cu–Au mineralization, and present H and O stable isotope data to constrain the origin of the Tongjing Cu–Au deposit.

2. Geologic setting

The Cretaceous Ningwu volcanic basin is located in the northern margin of the Yangtze Craton, east of the Tangcheng–Lujiang Fault (see Figs. 1 and 2 in Pan and Dong, 1999), and south of the Dabieshan ultrahigh-pressure metamorphic belt. The NNE-trending, rhomb-shaped, faulted volcanic basin (Ningwu Research Group, 1978; Fig. 1) is bound to the east by the Fangshan–Xiaodanyang Fault, to the west by the Yangtze River (Changjiang) Fault Zone, and to the north and south by the Nanjing–Hushu and Sanshanjie–Xuancheng faults (outside the limits of Fig. 1), respectively. The stratigraphic relationships within the Ningwu volcanic basin were described by Ningwu Research Group (1978); Mao et al. (2006), and Yu et al. (2011), and are summarized below.

The basement of the Ningwu volcanic basin consists of, from bottom to top, sedimentary rocks of the Lower–Middle Triassic Qinglong Group, the Upper Triassic Huangmaqing Formation, the Lower–Middle Jurassic Xiangshan Group, and the Upper Jurassic Xihengshan Formation (Ningwu Research Group, 1978). Volcanic rocks within the basin are subaerial and have been intruded by coeval subvolcanic plutons. The Ningwu basin hosts a 2.65-km-thick Cretaceous volcanic belt that is divided from bottom to top into the Longwangshan, Dawangshan, Gushan and Niangniangshan Formations. The Longwangshan Formation is dominated by lavas and pyroclastic rocks of hornblende-bearing basaltic andesite to andesite, and locally by trachyandesites. These volcanic rocks yield zircon U–Pb ages of 131–135 Ma (Zhang et al., 2003; Zhou et al., 2011). Andesitic volcanic rocks, tuffs, and lavas of the Dawangshan Formation are exposed in the northern and central parts of the volcanic basin, and have been dated at 127–132 Ma by zircon U–Pb methods (Zhang et al., 2003; Zhou et al., 2011). Andesites and pyroclastic counterparts of the Gushan Formation crop out in the southern (Zhongshan and Gushan) and northern (Meishan) parts of the volcanic basin, and have zircon U–Pb ages of 128–130 Ma (Zhou et al., 2011). Phonolites

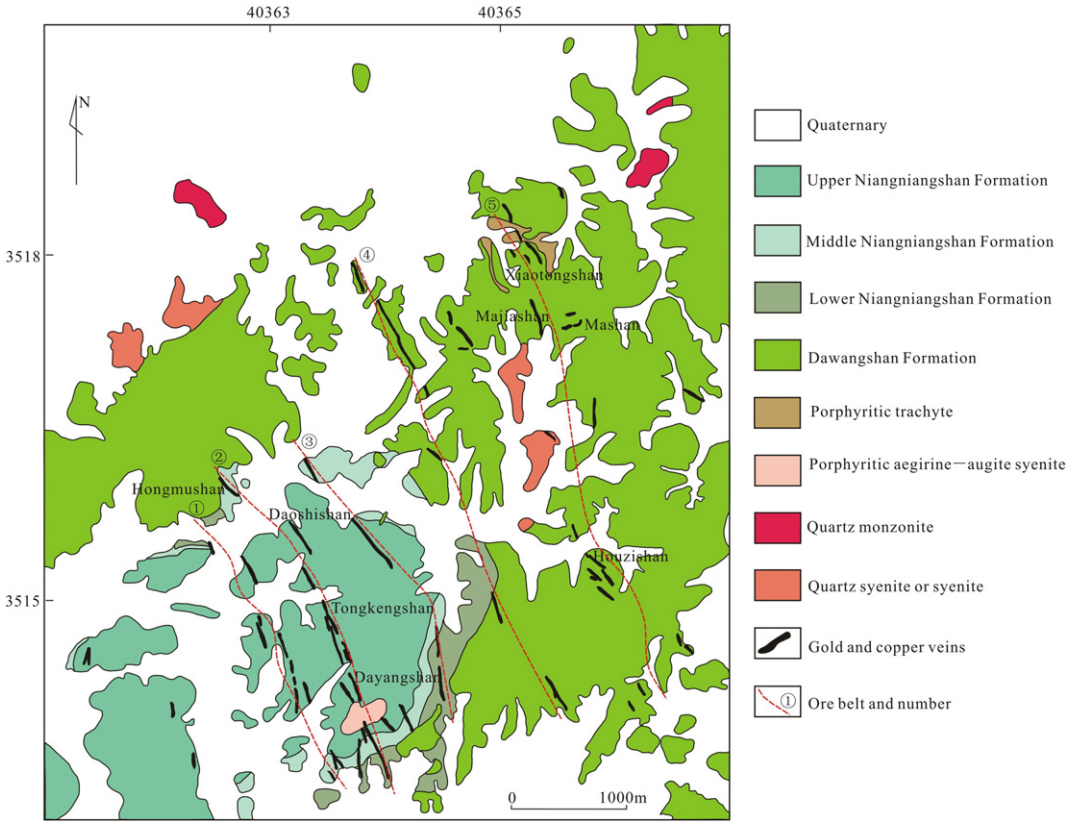

Fig. 2. Geological map of the Tongjing Cu–Au deposit. Modified from Jiangsu Geological Survey (2010).

and phonolitic tuffs of the Niangniangshan Formation define the Niangniangshan caldera (Fig. 1), and have been dated at 127–131 Ma by zircon U–Pb analysis (Yan et al., 2009a; Zhou et al., 2011). Subvolcanic plutons, emplaced shortly after the Dawangshan Formation volcanism, are widely distributed within the Ningwu basin, and include gabbro–diorite porphyries and/or pyroxene diorites that yield zircon U–Pb ages of ~130 Ma (Zhou et al., 2013). These subvolcanic rocks occur as stocks emplaced at depths of <1 km from the paleosurface, and are characterized by high concentrations of alkali elements and high Na/K values ($Na_2O + K_2O$ = 4.8–9.1 wt.%, Na_2O/K_2O = 1.5–5.0; Ningwu Research Group, 1978). There is consensus that the iron mineralization in the Ningwu district is genetically related to these subvolcanic plutons (Ningwu Research Group, 1978; Mao et al., 2006, 2011, 2012; Hou et al., 2009a, 2009b, 2010, 2011, 2012; Yu et al., 2011). Granites also intrude the volcanic basin (Fig. 1). These granites yield LA–ICP–MS zircon U–Pb ages of 130–126 Ma, and have low $\varepsilon_{Nd(t)}$ values (−2.33 to −7.25) and high initial $(^{87}Sr/^{86}Sr)_i$ ratios (0.704957–0.708725, Yuan et al., 2011). Geological data from the Ningwu basin suggest that the Cretaceous volcanic and subvolcanic rocks, and granitic rocks are developed along NE-striking fault zones (e.g., the Yangtze River fault zones) in east China, and likely formed in an extensional setting within the Yangtze Craton (Mao et al., 2006, 2011; Yuan et al., 2011; Zhou et al., 2013).

In addition to the four major fault zones mentioned above, several NE–SW and NW–SE- to WNW–ESE-trending faults are extensively developed within the Ningwu volcanic basin (Fig. 1).

There are two types of gold deposits within the Ningwu basin. The first type is exemplified by the Meishan deposit. The Cu–Au orebodies are peripheral to the Fe-oxide–apatite deposits and overlie the iron orebodies at Meishan. The ore-forming fluids associated with iron mineralization were derived mainly from magmatic fluids, and the late-stage ore-forming fluids related to Cu–Au mineralization may have formed by the introduction of cooler meteoric water to the system (Yu et al., 2015a, 2015b). The Fe-oxide–apatite and Cu–Au deposits at Meishan formed in a large-scale magmatic–hydrothermal system and are associated with subvolcanic rocks, consisting of gabbro–diorite porphyry of the Dawangshan Formation (Yu et al., 2015a, 2015b). The second type is represented by the Tongjing deposit, where the mineralization is associated with volcanic and subvolcanic rocks of the Niangniangshan Formation, including nosean-bearing aegirine–augite syenites, quartz syenites, and quartz monzonites (Fig. 2).

3. Geology of the Tongjing Cu–Au deposit

3.1. Stratigraphy and structural geology

The Tongjing deposit is hosted by Cretaceous volcanic rocks of the Dawangshan and Niangniangshan Formations (Fig. 2). The Dawangshan Formation consists of pyroxene andesite, trachyandesite and trachyandesitic tuff, whereas the Niangniangshan Formation and associated Niangniangshan caldera consist of a lower series of trachytic volcanic breccia, agglomerate, intercalated pseudo-leucite phonolite, and tuffaceous siltstone units; a middle unit of nosean-bearing welded phonolitic volcanic breccia; and upper units of nosean-bearing phonolite and phonolitic brecciated tuff. The subvolcanic rocks of the Niangniangshan Formation include porphyritic aegirine–augite syenite, porphyritic trachyte, quartz monzonite, quartz syenite, and syenite stocks (Fig. 2). The characteristic rocks of the Niangniangshan Formation include pseudo-leucite phonolite, nosean-bearing phonolite and phonolitic brecciated tuff, and trachytic volcanic breccia. The pseudo-leucite phonolite shows a porphyritic texture with a tuffaceous groundmass (Fig. 3a). The phenocrysts are pseudo-leucite and K-feldspar in a tuffaceous groundmass. Primary leucite has been completely replaced by sericite, K-feldspar and calcite, with minor apatite in a tuffaceous groundmass (Fig. 3b). The nosean-bearing phonolitic brecciated tuff is composed of fragments of volcanic rocks and crystal fragments of nosean, K-feldspar, and pyroxene in a tuffaceous groundmass (Fig. 3c, d). The trachytic volcanic breccia consists of fragments of volcanic rocks and crystal fragments of K-feldspar and plagioclase (Fig. 3e) in a tuffaceous groundmass. The aegirine–augite syenite intrudes nosean-bearing phonolite (Fig. 3f), indicating that the aegirine–augite syenite formed after the volcanic rocks of the Niangniangshan Formation. The Niangniangshan Formation has been dated by zircon U–Pb methods at 127–131 Ma (Yan et al., 2009a; Zhou et al., 2011; this reference).

The Tongjing Cu–Au deposit is associated with structures dominated by the Niangniangshan caldera and associated NW trending faults that host the mineralization within the deposit (Fig. 2).

3.2. Mineralization

The Tongjing Cu–Au deposit is divided into five ore belts (No. 1 to No. 5, Fig. 2).These ore belts are equidistant from each other. The dominant ore belts within the deposit are the No. 1 ore belt; the No. 2 ore belt, including the Hongmushan, Daoshishan, Tongkengshan, and Dayangshan ore sections; and the No. 5 ore belt, including the Xiaotongshan, Majiashan, Mashan, and Houzishan ore sections (Fig. 2). Almost all of these ore belts host NW-trending mineralized veins that dip steeply to either the SW or NE, with the exception of the Mashan section, where these veins strike NE and dip steeply to the SE. The main orebody within the No. 2 ore belt is 3000 m long, strikes at 330°–340°, dips steeply to the ENE or WSW, and has a vein-like or lenticular shape (Gao et al., 2015).

Individual mineralized veins within the five ore belts range in length from several tens of meters to 340 m, are 0.5–4.2 m thick, and have vertical extents of 15–133 m. Individual veins have average Cu and Au concentrations of 0.12–2.38 wt.% and 1.37–16.08 g/t, respectively (Jiangsu Geological Survey, 2010).

3.3. Ore types and mineralogy

Cu–Au ores within the Tongjing deposit are dominated by native gold, chalcopyrite, and pyrite, with lesser amounts of bornite, tetrahedrite, and chalcocite in a quartz, siderite, calcite, sericite, barite, and chalcedony gangue. The ore has veined and stockwork, brecciated, and disseminated structures. Veined and stockwork ores include (1) quartz–siderite–specularite–pyrite–chalcopyrite ores (Fig. 4a; Fig. 5a), (2) quartz–siderite–chalcopyrite–pyrite ores (Fig. 4b), (3) quartz–chalcopyrite–pyrite ores (Fig. 5b, c), and (4) quartz–bornite ores (Fig. 5d). The first three types of ores are the main ores. The brecciated ores contain fragments of altered andesite cemented by quartz, siderite, specularite, pyrite and chalcopyrite (Fig. 4a). The disseminated ores contain chalcopyrite and pyrite hosted by volcanic rocks of the Dawangshan and Niangniangshan Formations. Gold is present as native gold (Fig. 5c), has subhedral and anhedral microgranular textures, is generally 0.01 mm in size, and is distributed in between quartz and chalcopyrite. The ore minerals within the deposit are chalcopyrite, pyrite, specularite, and native gold, with lesser bornite, wittichenite, tennantite, sphalerite, and galena in a gangue assemblage of quartz, siderite, calcite, and sericite.

3.4. Wall-rock alteration

Wall-rock alteration includes extensive silicification, siderite alteration, carbonation, sericitization, and kaolinization, and is closely related to the Cu–Au mineralization. Jiangsu Geological Survey (2010) recognized a distinct zoning of alteration within the Mashan ore section that is composed of a kaolinite–barite zone at the surface, a deeper quartz–sericite zone, and a lower quartz–siderite–sulfide zone. The latter two alteration zones are 2–3 m wide and are associated with Cu–Au mineralization.

3.5. Stages of mineralization

Cross-cutting relationships and mineral associations within the deposit have enabled the identification of two stages of mineralization:

Fig. 3. Photographs and photomicrographs of the main rocks of the Niangniangshan Formation from the Tongjing Cu–Au deposit. (a) pseudo-leucite phonolite with porphyritic texture; (b) photomicrograph of the rock in (a), showing a leucite phenocryst completely replaced by sericite, K-feldspar and calcite, cross-polarized light; (c) nosean-bearing phonolitic brecciated tuff consisting of fragments of volcanic rock and crystal fragments set in a tuffaceous groundmass; (d) photomicrograph of the rock in (c), showing crystal fragments consisting of nosean, K-feldspar and pyroxene set in a tuffaceous groundmass, plane-polarized light; (e) trachytic volcanic breccia consisting of fragments of volcanic rocks and crystal fragments of K-feldspar and plagioclase set in a tuffaceous groundmass; (f) aegirine–augite syenite intruding nosean-bearing phonolite. Abbreviations: Plct–pseudo-leucite, Kfs–K-feldspar, Pl–plagioclase, Srt–sericite, Cal–calcite, Ap–apatite, F–fragment, Nsn–nosean, and Px–pyroxene.

(1) a quartz–siderite–sulfide stage (Stage 1) associated with the formation of chalcopyrite, pyrite, native gold (Fig. 4; Fig. 5a–c), and lesser wittichenite (Fig. 5d) in a quartz and siderite gangue; and (2) a quartz–bornite stage (Stage 2) that cuts Stage 1 chalcopyrite (Fig. 5d–e), and is associated with the formation of chalcopyrite and minor amounts of bornite, tennantite and sphalerite (Fig. 5f) in a quartz gangue. Stage 1 is the main mineralization stage. The mineral paragenesis of the Tongjing Cu–Au deposit is presented in Fig. 6.

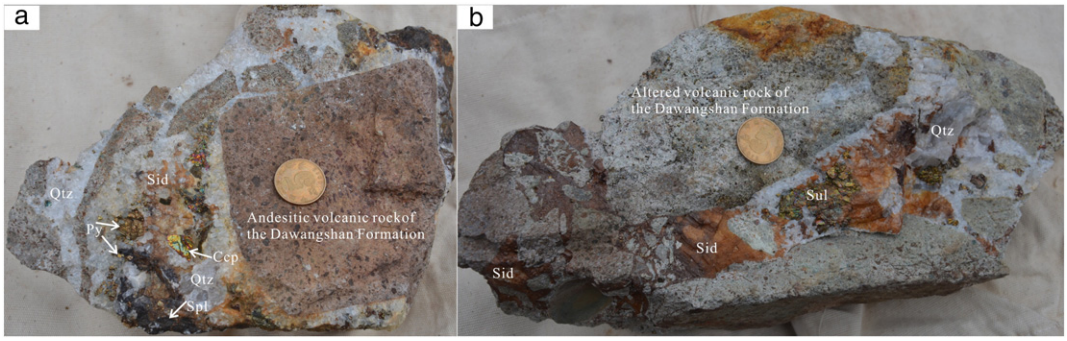

Fig. 4. Photographs of representative Stage 1 ores within the Mashan ore section of the Tongjing Cu–Au deposit: (a) quartz–siderite–specularite–chalcopyrite– pyrite vein crosscutting andesitic volcanic rock of the Dawangshan Formation; (b) quartz–siderit–sulfide vein crosscutting altered volcanic rock of the Dawangshan Formation. Abbreviations: Qtz–quartz, Spl–specularite, Py–pyrite, Ccp–chalcopyrite, Sul–sulfide, and Sid–siderite.

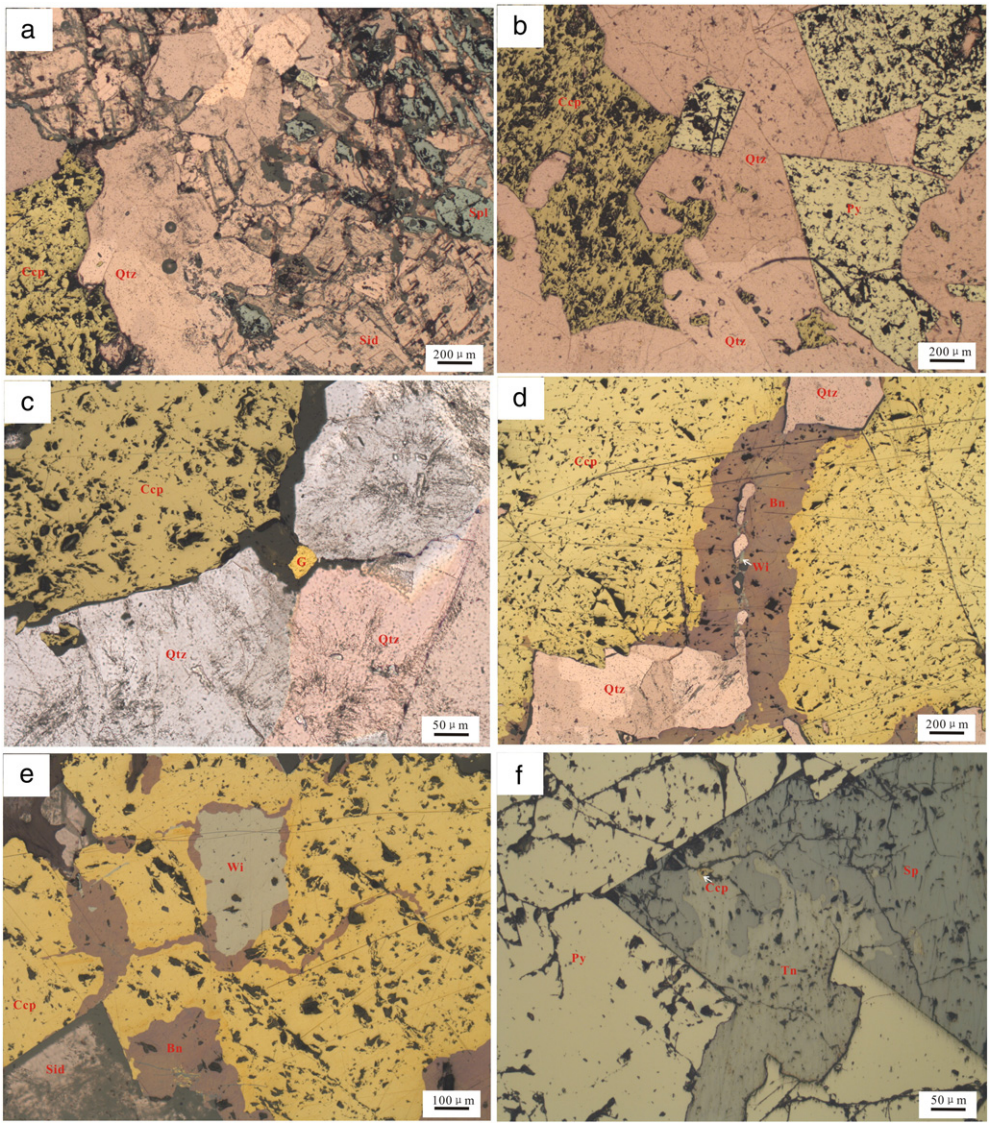

Fig. 5. Representative photomicrographs of the Tongjing Cu–Au deposit: (a) Stage 1 chalcopyrite coexisting with specularite, siderite and quartz; (b) Stage 1 chalcopyrite coexisting with pyrite and quartz; (c) Stage 1 chalcopyrite coexisting with quartz, and native gold distributed in the space between chalcopyrite and quartz; (d) Stage 2 quartz–bornite veinlet crosscutting Stage 1 chalcopyrite; (e) Stage 1 chalcopyrite coexisting with siderite and wittichenite, and Stage 2 bornite veinlet crosscutting chalcopyrite; (f) Stage 2 tennantite coexisting with pyrite and sphalerite. All photomicrographs were captured under combined reflected and transmitted light excepting for (f) (reflected light). Abbreviations: Bn–bornite, Wi–wittichenite, G–native gold, Tn–tennantite, Sp–sphalerite, and others are as Fig. 4.

4. Samples and analytical methods

4.1. Hydrogen and oxygen isotopes

Twelve quartz samples from the ores that formed in Stage 1 were used for hydrogen and oxygen isotope analysis. Mineral separation was carried out at the Langfang Geochemical Laboratory in Hebei Province, China. All mineral separates were examined using a binocular microscope prior to isotope analysis to ensure 99% purity.

H–O isotopes were analyzed using a Finnigan MAT253 mass spectrometer at the Analytical Laboratory of Beijing Research Institute of Uranium Geology, China National Nuclear Corporation, Beijing, China. Oxygen gas was produced by quantitatively reacting the samples with BrF_5 in externally heated nickel reaction vessels. Hydrogen was determined by quantitatively reacting the H_2O with Zn at high temperatures. The results are presented relative to SMOW, and have a precision of $\pm 1‰$ for δD and $\pm 0.2‰$ for $\delta^{18}O$.

4.2. Zircon U–Pb dating

Two samples (nosean-bearing phonolite and nosean-bearing phonolitic brecciated tuff) were collected from exposures in the Tongjing ore district for LA–MC–ICP–MS zircon U–Pb dating. Sample TJ-13-7 (118°33′26.76″E, 31°45′0.12″N) is a nosean-bearing phonolite. The phonolite is massive and porphyritic, and contains euhedral–subhedral tabular phenocrysts of K-feldspar (25%–40%), nosean (15%), clinopyroxene (5%–10%), and biotite (5%) set in a tuffaceous groundmass, with accessory apatite and magnetite. Sample TJ-13-62 (118°32′35.21″E, 31°44′46.48″N) is a nosean-bearing phonolitic brecciated tuff. It contains 15% volcanic rock fragments and 50% crystal fragments (feldspar, nosean, and clinopyroxene) set in a tuffaceous groundmass, with accessory apatite and magnetite. Before zircon separation, the volcanic rock fragments were removed from the sample.

Zircons were separated from an approximately 10 kg sample using conventional crushing and sieving techniques, and standard magnetic

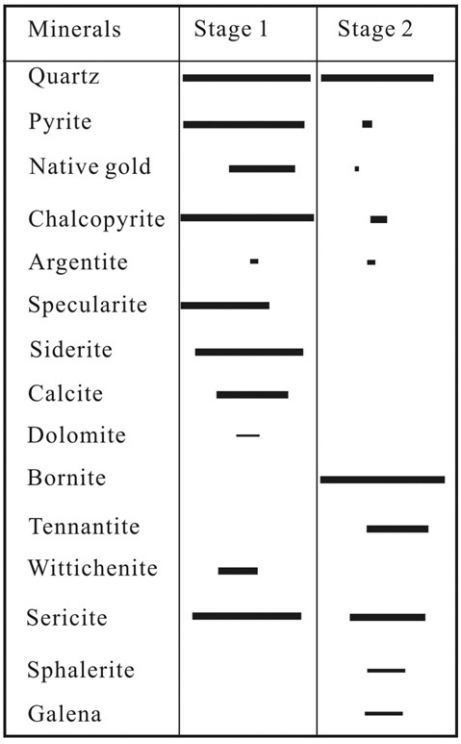

Fig. 6. Mineral paragenesis of the Tongjing Cu–Au deposit.

and heavy liquid separation, before purification using cold HF and HNO_3. Single zircons were hand-picked under a binocular microscope before mounting in epoxy resin. The sample mount was polished to expose the centers of individual zircons before examination under transmitted and reflected light and using cathodoluminescence (CL) imaging. CL imaging was undertaken at the Beijing Ion Microprobe Centre, Beijing, China, using a CAMECA SX–50 microprobe. U–Pb dating was undertaken by laser ablation multicollector inductively coupled plasma mass spectrometry (LA–MC–ICP–MS) at the Institute of Mineral Resources, Chinese Academy of Geological Sciences (CAGS), Beijing, China. Detailed operating conditions for the laser ablation system, the MC–ICP–MS instrument, and the data reduction approach are given in Hou et al. (2009a). Laser sampling was performed using a New Wave UP 213 laser ablation system, and a Thermo Finnigan Neptune MC–ICP–MS instrument was used to acquire ion-signal intensities. An array of four multi-ion-counters and three Faraday cups allowed for simultaneous detection of ^{202}Hg (on IC5), ^{204}Hg, ^{204}Pb (on IC4), ^{206}Pb (on IC3), ^{207}Pb (on IC2), ^{208}Pb (on L4), ^{232}Th (on H2), and ^{238}U (on H4) ion signals. Helium was used as a carrier gas, and argon was used as a make-up gas and mixed with the carrier gas via a T-connector before entering the ICP–MS. Each analysis incorporated a background acquisition of approximately 20–30 s (gas blank) followed by 30 s data acquisition from the sample. Off-line raw data selection, integration of background and analyte signals, time–drift corrections, and quantitative calibration for U–Pb dating were undertaken using the program ICPMSDataCal (Liu et al., 2010).

The Zircon GJ1 standard was used during external calibration of the U–Pb dating, and was analyzed twice every 5–10 analyses. Time–dependent U–Th–Pb isotopic ratio drifts were corrected using a linear interpolation (with time) for every 5–10 analyses, according to the variations in GJ1 (i.e., 2 zircon GJ1 analyses plus 5–10 unknown analyses plus 2 zircon GJ1 analyses; Liu et al., 2010). The U–Th–Pb isotopic ratios used for the GJ1 standard are those given by Jackson et al. (2004). The uncertainties on the preferred values used for the external GJ1 standard were propagated through calculations of the final uncertainties on these analyses. Common Pb corrections were not necessary as all analyzed zircons had low common ^{204}Pb signals and high ^{206}Pb/^{204}Pb ratios. U, Th, and Pb concentrations were calibrated using the zircon M127 standard with U = 923 ppm, Th = 439 ppm, and Th/U = 0.475 (Sláma et al., 2008). Concordia diagrams were constructed and weighted mean age calculations were made using the program Isoplot/Ex, version 3 (Ludwig, 1999). A plesovice standard zircon was also dated as an unknown sample and yielded a weighted mean ^{206}Pb/^{238}U age of 337 ± 2 Ma (2σ, n = 12), which is in good agreement with the recommended ^{206}Pb/^{238}U age of 337.13 ± 0.37 Ma (2σ; Sláma et al., 2008).

4.3. Ar–Ar dating

Sample TJ-13-120 was collected from an underground tunnel in the Mashan ore section for Ar–Ar dating of sericite. Sample TJ-13-120 is close to a Stage 1 siderite–quartz–sulfide vein, and is composed of quartz, sericite and pyrite (Fig. 7). The measured samples were crushed and purified by magnetic separator and then cleaned by ultrasonic treatment under ethanol. The purity of the sericite assemblage exceeded 99%. Samples were wrapped in aluminum foil and loaded into a tube of Al foil, together with two or three monitor samples. The tubes were sealed in a quartz bottle (40 mm high; 50 mm in diameter). The bottle was irradiated for 51 h 46 min in a nuclear reactor (The Swimming Pool Reactor, Chinese Institute of Atomic Energy, Beijing, China). The reactor delivers a neutron flux of 6.0×10^{12} n cm^{-2} s^{-1}. The integrated neutron flux is about 1.16×10^{18} n cm^{-2}. After irradiation, the samples and monitors were removed from the quartz bottle and then loaded into the vacuum extraction system. They were baked out for 48 h at 120–150 °C. The Ar extraction system comprised an electron bombardment heated furnace in which the samples were heated under vacuum. A thermocouple was used to monitor and control the temperature of the furnace. This furnace automatically attains the set temperature and remains within a range of a few degrees. The released gases are admitted to a purification system, with 30 min duration for heating–extraction for each temperature increment and 30 min for purification. The purification system uses a U-tube cooled with a mixture of acetone and dry ice, a titanium sublimation pump at a filament current of 38 A, and a titanium sponge furnace at 800 °C. Finally, the gases were purified by two Sorb-AC pumps at room temperature. Purified Ar was trapped by an activated charcoal finger at liquid-nitrogen temperature and then released into the Helix MC Mass Spectrometer for analysis of Ar isotopes at the Isotope Laboratory of

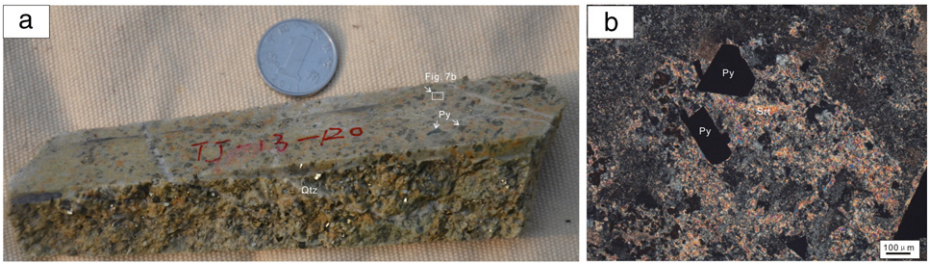

Fig. 7. (a) Photograph of silicification, sericitization and pyritization in sample TJ-13-120 from the Mashan ore section; (b) photomicrograph of the rock shown in (a). Abbreviations: Srt–sericite and others are as Fig. 4.

Table 1
Hydrogen and oxygen isotopic data for quartz from the Tongjing Cu–Au deposit.

Sample no.	Stage	$\delta^{18}O$ (‰)	T_h (°C)	δD (‰)	$\delta^{18}O_{fluid}$ (‰)	Sample location
MG-9	1	2.8	324	−61.3	−3.3	Majiashan ore section
DY-1	1	12.3	253	−89.9	3.5	Dayangshan ore section
DY-2	1	4.8	264	−81.7	−3.5	Dayangshan ore section
DY-4	1	8.8	229	−84.5	−1.2	Dayangshan ore section
DY-12	1	5.6	298	−81.6	−1.4	Dayangshan ore section
DY-13	1	6.1	222	−97.1	−4.3	Dayangshan ore section
DY-18	1	6.5	252	−84.6	−2.4	Dayangshan ore section
MG-6	1	9.5	252	−74.2	0.6	Majiashan ore section
MG-11	1	6.3	252	−63.9	−2.6	Majiashan ore section
MG-12	1	8.6	252	−65.6	−0.3	Majiashan ore section
MG-14	1	9	252	−57.7	0.1	Majiashan ore section
MG-19	1	10.4	252	−49.9	1.5	Majiashan ore section

the Institute of Geology, Chinese Academy of Geological Sciences, Beijing, China.

Measured isotopic ratios were corrected for mass discrimination, the atmospheric Ar component, blank levels, and irradiation-induced mass interference. The correction factors for interfering isotopes produced during irradiation were determined by analysis of irradiated K_2SO_4 and CaF_2, and have the following values: $(^{36}Ar/^{37}Ar)_{Ca} = 0.0002389$, $(^{40}Ar/^{39}Ar)_K = 0.004782$, and $(^{39}Ar/^{37}Ar)_{Ca} = 0.000806$. The blanks for m/e = 40, m/e = 39, m/e = 37, and m/e = 36 are $<6 \times 10^{-15}$ mol, 4×10^{-16} mol, 8×10^{-17} mol, and 2×10^{-17} mol, respectively. The decay constant used is $\lambda = 5.543 \times 10^{-10}$ a^{-1} (Steiger and Jager, 1977). All ^{37}Ar analyses were corrected for radiogenic decay (half-life of 35.1 days). Uncertainty in each apparent age is given at one standard deviation. The monitor used in this work is an internal standard of Fangshan biotite granite (ZBH-25) with an age of 132.7 ± 1.2 Ma and a potassium content of 7.579 ± 0.030 wt.% (Wang, 1983). The ISOPLOT/Ex program (ver. 3.0, Ludwig, 2003) was used for the $^{40}Ar/^{36}Ar$ vs. $^{39}Ar/^{36}Ar$ isochron and inverse isochron diagrams.

5. Results

5.1. Hydrogen and oxygen isotopes

Hydrogen and oxygen isotopic compositions for 12 handpicked quartz crystals from the Tongjing Cu–Au deposit are listed in Table 1. The measured $\delta^{18}O$ values are 2.8‰ to 10.4‰ for quartz. $\delta^{18}O_{H2O}$ values of the fluids are estimated at between −4.3‰ and 3.5‰, using the quartz–water fractionation equations (Clayton, 1972) and the temperature calculated from the fluid inclusion data (Yu et al., 2015b). All the quartz grains separated for $\delta^{18}O$ analyses were also analyzed for their hydrogen isotopic compositions. The δD values for fluid inclusion water in quartz range between −97.1‰ and −49.9‰.

5.2. Zircon U–Pb and sericite Ar–Ar dating

Although some zircons from the nosean-bearing phonolite and nosean-bearing phonolitic brecciated tuff at Tongjing were broken during zircon separation, zircons with well-developed magmatic oscillatory zoning (Fig. 8), low numbers of inclusions, and without bright rims or fissures were chosen for U–Pb dating. Zircons in the nosean-bearing phonolite (TJ-13-7) at Tongjing are euhedral and prismatic, 100–180 μm long and 65–100 μm wide, and show oscillatory zoning, indicating a magmatic origin. Twenty analyses of 20 zircons from sample TJ-13-7 were obtained, and the LA–MC–ICP–MS U–Pb data for these zircons are summarized in Table 2. These analyses yield a concordant age of 129.8 ± 0.5 Ma (n = 20, MSWD = 4.6; Fig. 9a). Uranium concentrations range from 108.6 to 2297 ppm and thorium concentrations range from 100.1 to 2060 ppm. The Th/U ratios are relatively high, ranging from 0.7 to 2.69, except for spot 16 (Th/U = 0.15), indicating their magmatic origin (Hoskin and Black, 2000). Therefore, the weighted mean $^{206}Pb/^{238}U$ age of 129.8 ± 0.5 Ma (MSWD = 4.6) in this study is interpreted as the crystallization age of the nosean-bearing phonolite at Tongjing.

Zircons from the nosean-bearing phonolitic brecciated tuff (TJ-13-62) at Tongjing are 150–220 μm long and 90–210 μm wide. They are dominantly euhedral, prismatic, and colorless, and show oscillatory zoning (Fig. 8b). These features indicate a magmatic origin (Hoskin and Black, 2000), as also suggested by their Th/U ratios (0.37–2.58). All 15 analyses of igneous zircons from sample TJ-13-62 (summarized in Table 2) were carried out using the LA–MC–ICP–MS U–Pb method

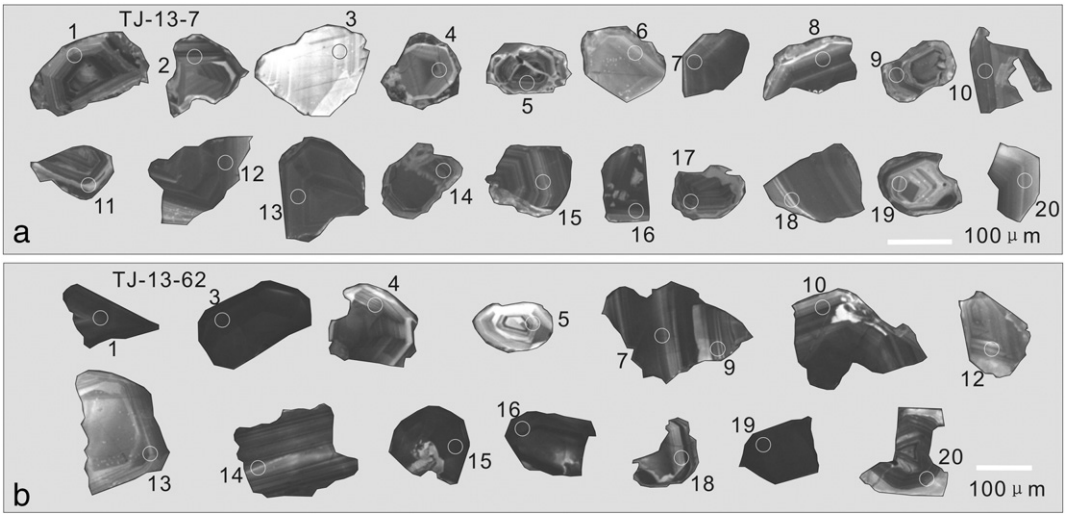

Fig. 8. Cathodoluminescence images of zircons from (a) nosean-bearing phonolite and (b) nosean-bearing phonolitic brecciated tuff at Tongjing. Analyzed spots are circled.

Table 2
LA–MC–ICP–MS zircon U–Pb data for the nosean-bearing phonolite and nosean-bearing phonolitic brecciated tuff from the Tongjing Cu–Au deposit.

Spot	Pb/ppm	Th/ppm	U/ppm	Th/U	$^{207}Pb/^{206}Pb$	1σ	$^{207}Pb/^{235}U$	1σ	$^{206}Pb/^{238}U$	1σ	$^{207}Pb/^{206}Pb$/Ma	1σ	$^{207}Pb/^{235}U$/Ma	1σ	$^{206}Pb/^{238}U$/Ma	1σ
TJ-13-7 nosean-bearing phonolite																
TJ-13-7-1	16	473	673	0.70	0.05060	0.00238	0.14434	0.00662	0.02075	0.00028	233	109	137	6	132	2
TJ-13-7-2	14	564	565	1.00	0.05082	0.00291	0.14606	0.00803	0.02099	0.00029	232	133	138	7	134	2
TJ-13-7-3	3	100	109	0.92	0.05038	0.00514	0.13705	0.01241	0.02080	0.00067	213	222	130	11	133	4
TJ-13-7-4	24	1437	803	1.79	0.05125	0.00264	0.14394	0.00706	0.02049	0.00034	254	119	137	6	131	2
TJ-13-7-5	29	1111	1156	0.96	0.04817	0.00189	0.13715	0.00549	0.02062	0.00028	109	93	130	5	132	2
TJ-13-7-6	10	653	320	2.04	0.04777	0.00474	0.13640	0.01416	0.02051	0.00047	87	222	130	13	131	3
TJ-13-7-7	27	2060	766	2.69	0.04875	0.00212	0.13513	0.00537	0.02024	0.00025	200	102	129	5	129	2
TJ-13-7-8	20	1514	576	2.63	0.05235	0.00246	0.14443	0.00666	0.02011	0.00030	302	107	137	6	128	2
TJ-13-7-9	32	1346	1217	1.11	0.04904	0.00174	0.13682	0.00485	0.02024	0.00026	150	83	130	4	129	2
TJ-13-7-10	10	539	322	1.68	0.05089	0.00733	0.13987	0.01788	0.02068	0.00110	235	304	133	16	132	7
TJ-13-7-11	20	609	830	0.73	0.04803	0.00208	0.13477	0.00576	0.02037	0.00029	102	109	128	5	130	2
TJ-13-7-12	12	758	374	2.03	0.04796	0.00273	0.13178	0.00713	0.02013	0.00035	98	135	126	6	128	2
TJ-13-7-13	27	1907	764	2.50	0.05246	0.00212	0.14537	0.00558	0.02021	0.00029	306	93	138	5	129	2
TJ-13-7-14	16	795	560	1.42	0.05379	0.00351	0.14846	0.01010	0.01999	0.00034	361	146	141	9	128	2
TJ-13-7-15	10	460	331	1.39	0.04769	0.00366	0.13238	0.01032	0.02023	0.00034	83	174	126	9	129	2
TJ-13-7-16	50	343	2297	0.15	0.05131	0.00404	0.14100	0.01073	0.01992	0.00034	254	186	134	10	127	2
TJ-13-7-17	34	1166	1255	0.93	0.05367	0.00249	0.14907	0.00704	0.02010	0.00029	367	101	141	6	128	2
TJ-13-7-18	7	328	191	1.72	0.05725	0.01367	0.15814	0.02960	0.02098	0.00116	502	453	149	26	134	7
TJ-13-7-19	7	212	284	0.75	0.04677	0.00563	0.13333	0.01702	0.02071	0.00070	39	263	127	15	132	4
TJ-13-7-20	8	283	322	0.88	0.04942	0.00439	0.13303	0.01167	0.01962	0.00060	169	193	127	10	125	4
TJ-13-62 nosean-bearing phonolitic brecciated tuff																
TJ-13-62-1	17	501	718	0.70	0.04750	0.00207	0.12743	0.00511	0.02006	0.00053	76	100	122	5	128	3
TJ-13-62-3	60	2863	2152	1.33	0.04935	0.00135	0.13705	0.00349	0.02018	0.00023	165	65	130	3	129	1
TJ-13-62-4	7	425	249	1.70	0.05065	0.00408	0.13840	0.01068	0.02027	0.00039	233	217	132	10	129	2
TJ-13-62-5	5	165	210	0.79	0.05239	0.00321	0.14685	0.00864	0.02075	0.00035	302	134	139	8	132	2
TJ-13-62-7	39	2699	1172	2.30	0.04994	0.00151	0.13972	0.00427	0.02028	0.00027	191	70	133	4	129	2
TJ-13-62-9	25	1703	716	2.38	0.05237	0.00207	0.14389	0.00501	0.02020	0.00030	302	91	137	4	129	2
TJ-13-62-10	31	2317	899	2.58	0.05217	0.00189	0.14439	0.00509	0.02019	0.00027	300	81	137	5	129	2
TJ-13-62-12	13	690	440	1.57	0.05454	0.00311	0.14666	0.00775	0.01984	0.00032	394	128	139	7	127	2
TJ-13-62-13	7	214	266	0.81	0.05393	0.00317	0.14844	0.00881	0.02023	0.00032	369	131	141	8	129	2
TJ-13-62-14	15	891	511	1.74	0.04922	0.00221	0.13708	0.00623	0.02031	0.00029	167	106	130	6	130	2
TJ-13-62-15	64	2709	2397	1.13	0.04860	0.00101	0.13982	0.00297	0.02083	0.00020	128	48	133	3	133	1
TJ-13-62-16	73	2848	2912	0.98	0.04883	0.00119	0.13465	0.00333	0.01992	0.00016	139	56	128	3	127	1
TJ-13-62-18	38	2471	1280	1.93	0.04627	0.00221	0.12612	0.00544	0.01982	0.00024	13	111	121	5	127	2
TJ-13-62-19	66	1124	3060	0.37	0.04519	0.00131	0.12676	0.00360	0.02028	0.00019	–	–	121	3	129	1
TJ-13-62-20	18	553	775	0.71	0.05171	0.00297	0.14072	0.00781	0.01975	0.00044	272	99	134	7	126	3

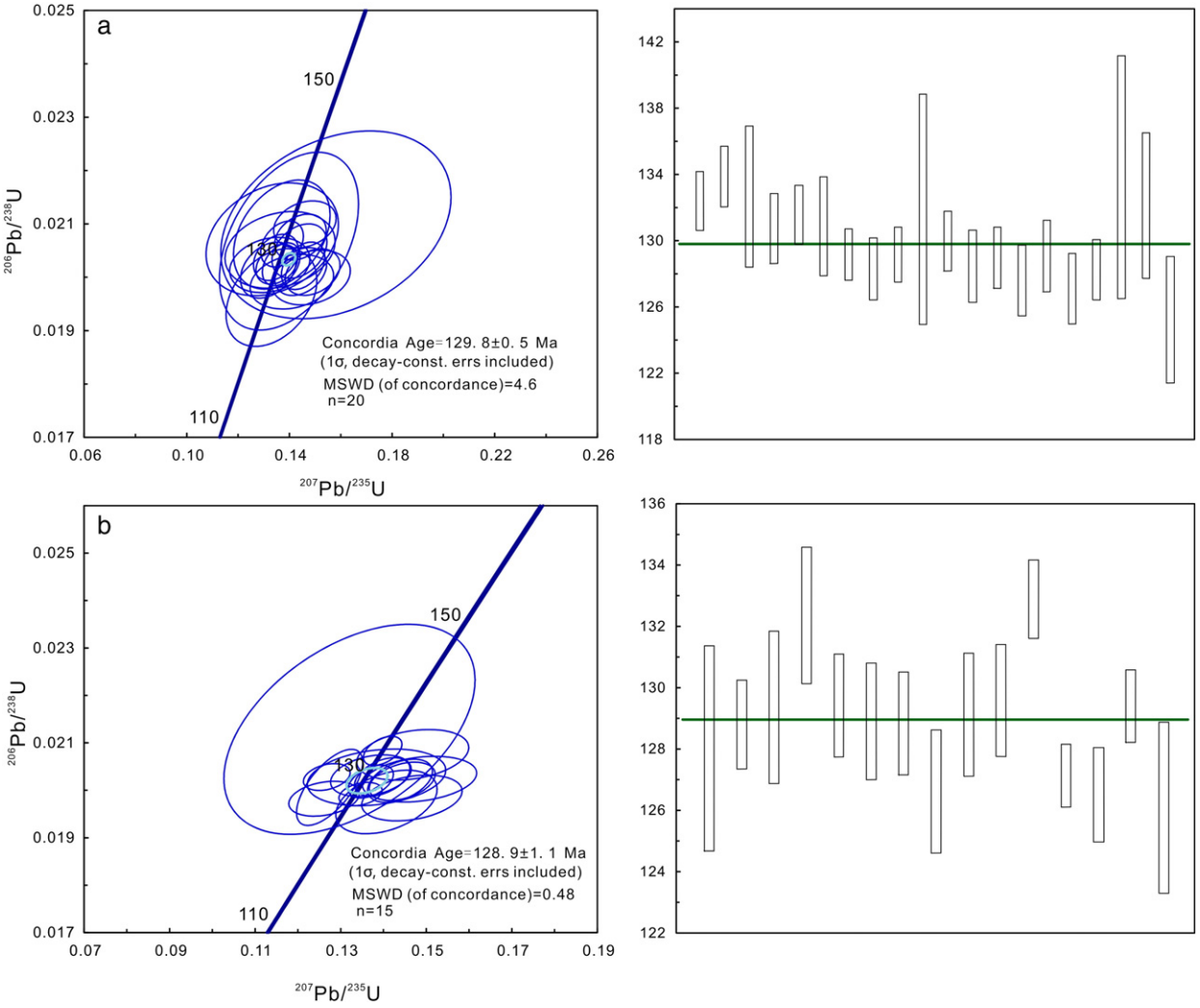

Fig. 9. LA–MC–ICP–MS zircon U–Pb ages of zircon for (a) the nosean-bearing phonolite and (b) the nosean-bearing phonolitic brecciated tuff at Tongjing.

and yield excellent concordant results with a weighted mean $^{206}Pb/^{238}U$ age of 128.9 ± 1.1 Ma (n = 15, MSWD = 0.48; Fig. 9b). This age is interpreted to represent the crystallization age of the nosean-bearing phonolitic brecciated tuff (TJ-13-62) at Tongjing.

Sericite from sample TJ-13-120 at Tongjing was analyzed for $^{40}Ar–^{39}Ar$ dating, and the results are listed in Table 3 and presented graphically in Fig. 10. Plateau ages were determined using the criteria of Dalrymple and Lamphere (1971), which specify the presence of at least three continuous incremental heating steps with statistically indistinguishable ages, and which constitute about 65% of the total ^{39}Ar released during the experiment. The first two steps from sample TJ-13-120 have young apparent ages (Fig. 10) that are indicative of reactor-induced ^{39}Ar recoil (Muecke et al., 1988; Chen et al., 2010). The sericite assemblage (sample TJ-13-120) at Tongjing yields a well-defined plateau age of 131.3 ± 1.3 Ma, which is composed of 8 consecutive steps from 770 °C to 1, 080 °C, accounting for 67.6% of the gas released (Fig. 10a

Table 3
$^{40}Ar–^{39}Ar$ data for sericite from the Tongjing Cu–Au deposit.
Sample: TJ-13-120, W = 30.28 mg, J = 0.004362.

Step	T (°C)	$(^{40}Ar/^{39}Ar)_m$	$(^{36}Ar/^{39}Ar)_m$	$(^{37}Ar/^{39}Ar)_m$	$(^{38}Ar/^{39}Ar)_m$	^{40}Ar (%)	$^{40}Ar^*/^{39}Ar$	^{39}Ar ($\times10^{-14}$ mol)	^{39}Ar (% of cum.)	Age (Ma) (±1σ)
1	700	9.7506	0.0241	0.0425	0.0170	26.89	2.6224	1.80	7.90	20.52 ± 0.41
2	740	16.8163	0.0046	0.0009	0.0132	91.83	15.4430	5.52	32.09	117.6 ± 1.1
3	770	18.6185	0.0037	0.0087	0.0130	94.09	17.5182	5.08	54.37	132.8 ± 1.3
4	790	18.5216	0.0034	0.0201	0.0130	94.52	17.5071	3.37	69.15	132.8 ± 1.3
5	810	18.4376	0.0034	0.0275	0.0129	94.54	17.4307	2.46	79.95	132.2 ± 1.3
6	830	18.5211	0.0042	0.0073	0.0128	93.33	17.2851	1.33	85.79	131.1 ± 1.3
7	860	18.7421	0.0054	0.0128	0.0131	91.40	17.1307	0.89	89.67	130.0 ± 1.3
8	910	19.2759	0.0069	0.0610	0.0135	89.39	17.2309	1.26	95.19	130.7 ± 1.3
9	980	19.2043	0.0064	0.0313	0.0135	90.21	17.3255	0.74	98.43	131.4 ± 1.4
10	1080	23.8718	0.0239	0.2528	0.0178	70.51	16.8362	0.29	99.71	127.8 ± 1.7
11	1400	90.4105	0.2582	0.7682	0.0684	15.68	14.1810	0.07	100.00	108 ± 10

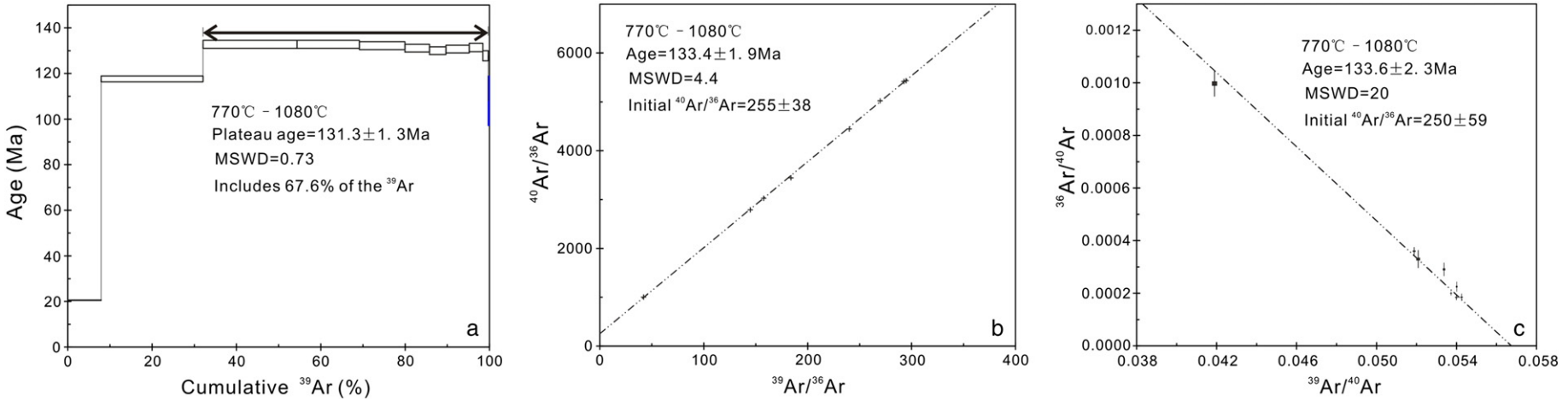

Fig. 10. (a) Plateau, (b) isochron, and (c) inverse isochron ^{40}Ar–^{39}Ar ages of sericite from the Tongjing Cu–Au deposit.

and Table 3). This age is also identical, within uncertainty, to the isochron age of 133.4 ± 1.9 Ma (Fig. 10b) and the inverse isochron age of 133.6 ± 2.3 Ma (Fig. 10c) for the sericite (sample TJ-13-120) (see Table 3).

6. Discussion

6.1. Source of ore fluids

The ore-forming fluids of the Tongjing Cu–Au deposit had moderate temperatures (210–270 °C) and moderate salinities (12–22 wt.% NaCl equiv., Yu et al., 2015b). Oxygen and hydrogen isotope systematics can be used to constrain the source of the ore-forming hydrothermal fluids (Clayton, 1972). The δD_{H2O} values of quartz that formed during the main stage of mineralization (Stage 1) in the Tongjing Cu–Au deposit vary from −97.1‰ to −49.9‰ (Table 1). Six samples fall in the range of magmatic water (−80‰ to −40‰) as defined by Sheppard (1986). Five samples have δD_{H2O} values of −81.6‰ to −89.9‰ (Table 1), which are slightly lower than that of magmatic water, whereas one sample has a δD_{H2O} value of −97.1‰ (Table 1), which is significantly lower than that of magmatic water. Using the fractionation equation of quartz from Clayton (1972) and the average homogenization temperature of fluid inclusions in quartz, the calculated $\delta^{18}O_{fluid}$ values of quartz range from −4.3‰ to 3.5‰ (Table 1). These values are much lower than that of magmatic water (5.5‰–9.5‰; Sheppard, 1986) and have the hydrothermal characteristics of meteoric water with a $\delta^{18}O$ drift, as defined by Zhang et al. (2011). On a plot of δD versus $\delta^{18}O_{fluid}$ (Fig. 11), all analyses fall outside the magmatic water field, indicating that the ore fluids of Stage 1 in the Tongjing deposit were derived mainly from meteoric fluids. An alternative interpretation is that the ore-forming fluids derived from early magmatic fluids experienced oxygen isotopic exchange with meteoric water during Stage 1 mineralization.

The sulfur isotopic compositions of the pyrite and chalcopyrite that formed in Stage 1 were presented by Yu et al. (2015b). A total of 29 sulfides that formed in Stage 1 yielded $\delta^{34}S$ values from 0.4‰ to 4.7‰, with a mean of 3.0‰ (Yu et al., 2015b), reflecting the derivation of sulfur from a single source, most probably magmatic. The Cu–Au mineralization is related to the volcanic rocks and corresponding subvolcanic rocks in the Niangniangshan Formation, as suggested by the sulfur isotopes, hydrogen and oxygen isotopes, and fluid inclusions.

6.2. Ages of the volcanic rocks and associated mineralization

The Rb–Sr isochron age of K-feldspar, plagioclase, biotite, and a nosean-bearing phonolite whole-rock sample of the Niangniangshan Formation is 133.1 ± 3.2 Ma (Yan et al., 2009b). The Niangniangshan Formation has been dated by the zircon U–Pb method at 127–131 Ma (Yan et al., 2009a; Zhou et al., 2011). LA–MC–ICP–MS zircon U–Pb ages in this study indicate that the nosean-bearing phonolite and nosean-bearing phonolitic brecciated tuff of the Niangniangshan Formation at Tongjing were formed at 129.8 ± 0.5 Ma and 128.9 ± 1.1 Ma, respectively. These results are similar to those presented by Yan et al. (2009a) and Zhou et al. (2011), and confirm that mineralization-related volcanic rocks of the Niangniangshan Formation at Tongjing were erupted at ~130 Ma, contemporaneously with the mineralization.

Many studies have shown that ^{40}Ar–^{39}Ar dating of mica can be used to reliably date hydrothermal ore deposits (Peng et al., 2006; Li et al., 2008; Xie et al., 2012). Homogenization temperatures of fluid inclusions in quartz and siderite at Tongjing range from 210 °C to 270 °C (Yu et al., 2015b), lower than the closure temperature of argon isotopes in mica (~300–350 °C, McDougall and Harrison, 1999). However, the sericite coexists with pyrite and quartz at Tongjing (Fig. 7). Therefore, the well-defined plateau age (131.3 ± 1.3 Ma) of the sericite sample constrains the timing of formation of pyrite and associated gold mineralization in the Tongjing deposit. This age is indistinguishable, within analytical error, from the LA–MC–ICP–MS zircon U–Pb ages (128.9 ± 1.1–129.8 ± 0.5 Ma) of the associated nosean-bearing phonolite and nosean-bearing phonolitic brecciated tuff of the Niangniangshan Formation. The excellent agreement between the U–Pb and ^{40}Ar–^{39}Ar age data confirms a genetic link between the volcanism and Cu–Au mineralization.

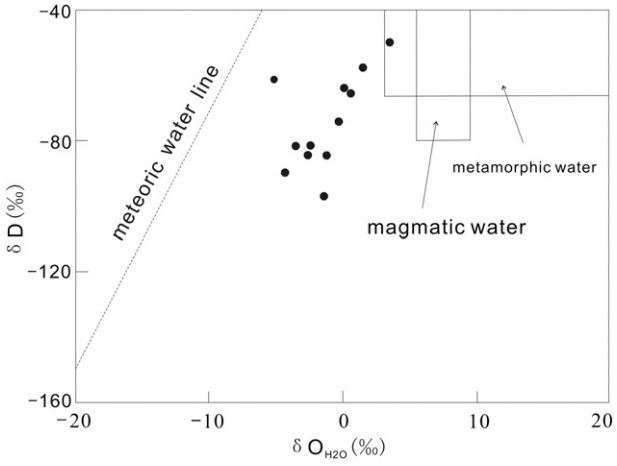

Fig. 11. δD vs. $\delta^{18}O_{fluid}$ diagram for quartz in the Tongjing deposit. After Sheppard (1986).

6.3. Genetic model

The sulfur in the Cu–Au ores was mainly of magmatic origin (Yu et al., 2015b). The ore-forming fluids were derived mainly from magmatic water that had experienced isotopic exchange with meteoric water during mineralization, as suggested by the H–O isotopic compositions (Fig. 11) and the ages of the volcanic rocks of the Niangniangshan Formation and associated mineralization.

The parental magma that formed the Niangniangshan Formation was generated by partial melting of the lithospheric mantle, and this magma assimilated minor upper-crustal material during ascent (Wang et al., 2006; Wang, 2009). The K-rich volcanic rocks of the Niangniangshan Formation were formed by fractional crystallization and emplaced into the pyroxene andesites of the Dawangshan Formation. At the same time, a crater and associated faults were formed. These faults provided deposition sites for Cu–Au mineralization (Fig. 12).

In the Early Cretaceous, the subvolcanic plutons, including porphyritic aegirine–augite syenite, porphyritic trachyte, quartz monzonite, quartz syenite, and syenite stocks, intruded the volcanic rocks of the Dawangshan and Niangniangshan Formations (Fig. 2). We envisage that the ore-forming fluids derived from the subvolcanic plutons and corresponding volcanic rocks of the Niangniangshan Formation migrated upwards along faults to higher levels and reacted with the volcanic rocks to form the Cu–Au mineralization and associated alteration. The capacity to transport metallic components is directly related to the physicochemical properties of the ore-forming fluid (Layne and Spooner, 1991; Hemley et al., 1992). Previous studies have noted that Cu and Au show significant enrichment in the fluid phases separated from melts and that the partitioning process is strongly affected by the H_2O content and chlorine concentration in the magma (Urabe, 1985; Candela and Holland, 1994). Zhou et al. (2007) suggested that declines in temperature and salinity caused by cooling and mixing is the main trigger of Cu deposition, whereas declines in pH, $m_{\Sigma S}$ and fO_2 caused by fluid boiling and mixing trigger Au deposition, based on geochemical data for Yueshan Cu–Au skarn- and vein-type deposits. Here, we infer that the ore-forming fluids derived from the subvolcanic plutons and corresponding volcanic rocks provided most of the ore-forming components in the Tongjing Cu–Au deposit (Fig. 12). Mixing of magmatic and meteoric water in the quartz–siderite–sulfide stage and the quartz–bornite stage led to more rapid cooling and dilution of the hot ore-

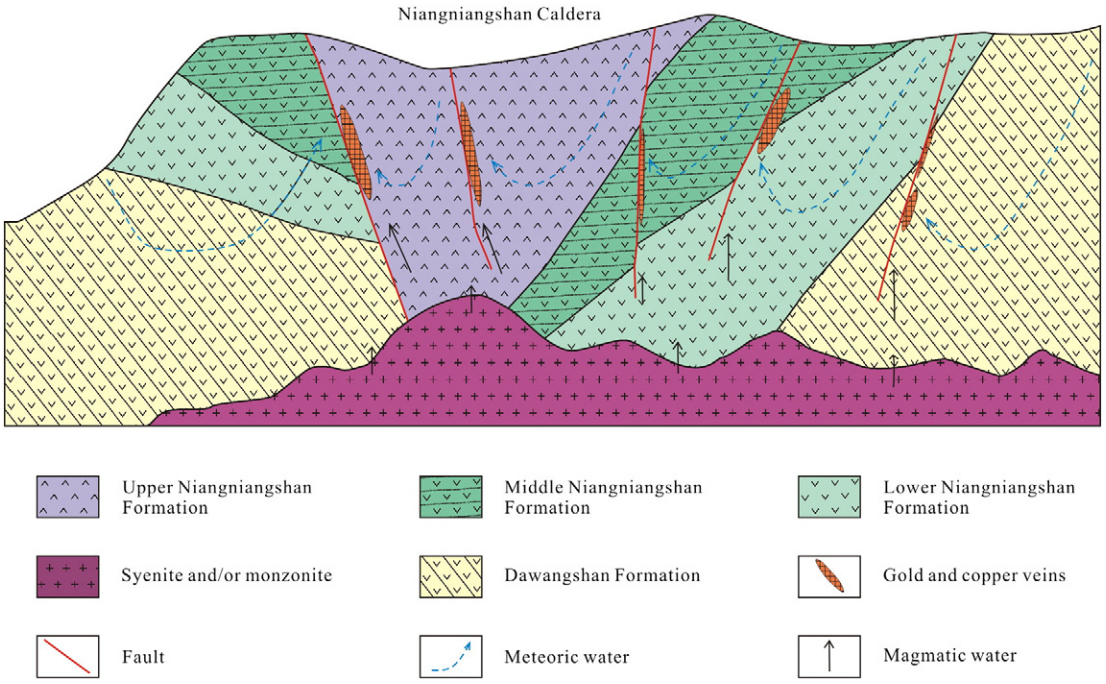

Fig. 12. Schematic diagrams illustrating the proposed genetic model for the Tongjing Cu–Au deposit.

forming fluids, resulting in the precipitation of copper and gold in quartz and siderite veins, and the formation of the Tongjing Cu–Au deposit. Further research is required to determine the nature of the fluid of the quartz–bornite stage. Cu–Au mineralization in the Tongjing ore district is temporally and genetically associated with the volcanic and subvolcanic rocks of the Niangniangshan Formation.

6.4. Comparison with other alkaline intrusion-related gold deposits

In recent years, gold deposits of considerable size that are associated with alkaline intrusions have been discovered at Dongping, Hebei Province (Bao et al., 2014), at Yao'an, Yunnan Province (Bi et al., 2004), and at Guilaizhuang, Shandong Province (Xu et al., 2014) in China. The discovery of these gold deposits prompted major research into the association between gold mineralization and alkaline intrusions. Some researchers argue that there is no direct genetic association between gold deposits and alkaline intrusions, but that both share the same regional tectonic setting (Wyman and Kerrich, 1988). However, it has also been suggested that such deposits form over several stages, with the mineralizing fluids of the earliest stage being regarded as magmatic and originating from the alkaline magmatic system (Jensen and Barton, 2000). These deposits form in a variety of tectonic settings, most notably in arc environments and in areas of extensional tectonics (Jensen and Barton, 2000).

The Tongjing Cu–Au deposits in the Ningwu basin are genetically and possibly tectonically similar to alkaline intrusion-related gold deposits elsewhere in the world. The Tongjing hydrothermal system is characterized by a temporal and genetic relationship between mineralization and alkaline magmatism, with the mineralizing fluids of the earliest stage being magmatic and originating from the alkaline magmatic system (Jensen and Barton, 2000), as suggested by the sulfur isotopes, fluid inclusions (Yu et al., 2015b), H–O isotopic compositions and ages of the mineralization and associated volcanic and subvolcanic rocks of the Tongjing Cu–Au deposit. The Niangniangshan Formation and associated Cu–Au mineralization formed in an intra-continental extensional setting (Wang et al., 2006), where partial melting of lithospheric mantle was likely controlled by lithospheric thinning and upwelling of hot asthenosphere along major NE–SW-striking fault zones (e.g., the Tanlu and Yangtze River fault zones).

7. Conclusions

(1) The Tongjing Cu–Au deposit is hosted in the Dawangshan and Niangniangshan Formations, and contains vein orebodies. The wall-rock alteration is dominated by silicification, siderite alteration, carbonation, sericitization, chloritization, and kaolinization. The ore-forming process comprised a quartz–siderite–sulfide stage (Stage 1) and a quartz–bornite stage (Stage 2). The siderite–quartz–sulfide stage was the main stage of mineralization.

(2) The ore-forming fluids were derived from early magmatic fluids and may have experienced oxygen isotopic exchange with meteoric water during the quartz–siderite–sulfide stage.

(3) The nosean-bearing phonolite and nosean-bearing phonolitic brecciated tuff yield zircon LA–MC–ICP–MS U–Pb ages of 129.8 ± 0.5 Ma (MSWD = 4.6) and 128.9 ± 1.1 Ma (MSWD = 0.48), respectively. Sericite gives a ^{40}Ar–^{39}Ar age of 131.3 ± 1.3 Ma (MSWD = 0.73), suggesting that the mineralization formed during the Early Cretaceous. The geological and geochemical evidence presented in this paper suggests that the Tongjing Cu–Au deposit is a volcanic–subvolcanic hydrothermal deposit that is spatially, temporally, and genetically related to the volcanic and subvolcanic rocks of the Niangniangshan Formation.

Acknowledgements

We thank Huang Jianping, Sun Xihua, Qian Lingyu, and Wang Lijuan for support and assistance during fieldwork. This work was financially supported by the National Natural Science Foundation of China (41372091) and a State Key Fundamental Program project (2012CB416803). We gratefully acknowledge constructive comments and helpful suggestions from Professor Franco Pirajno and two anonymous reviewers that improved earlier versions of the manuscript.

References

Bao, Z., Sun, W., Li, C., Zhao, Z., 2014. U–Pb dating of hydrothermal zircon from the Dongping gold deposit in North China: constraints on the mineralization processes. Ore Geol. Rev. 61, 107–119.

Bi, X., Hu, R., Cornell, D.H., 2004. The alkaline porphyry associated Yao'an gold deposit, Yunnan, China: rare earth element and stable isotope evidence for magmatic-hydrothermal ore formation. Mineral. Deposita 39, 21–30.

Candela, P.A., Holland, H.D., 1994. The partitioning of copper and molybdenum between silicate and melts and aqueous fluids. Geochim. Cosmochim. Acta 48, 373–380.

Chang, Y.F., Liu, X.P., Wu, Y.C., 1991. The Copper–Iron Belt of the Lower and Middle Reaches of the Changjiang River. Geological Publishing House, Beijing, pp. 1–379 (in Chinese with English abstract).

Chen, Y.C., Sheng, J.F., Ai, Y.D., 1981. Meishan iron deposit—an ore magmahydrothermal deposit. Bull. Inst. Miner. Deposits, Chin. Acad. Geol. Sci. 2, 26–48 (in Chinese with English abstract).

Chen, H., Clark, A.H., Kyser, T.K., Ullrich, T.D., Baxter, R., Chen, Y., Moody, T.C., 2010. Evolution of the Giant Marcona-Mina Justa Iron Oxide-Copper-Gold District, South-Central Peru. Econ. Geol. 105, 155–185.

Clayton, R.N., 1972. Oxygen isotope exchange between quartz and water. J. Geophys. Res. 77, 3057–3607.

Dalrymple, G.B., Lamphere, M.A., 1971. $^{40}Ar/^{39}Ar$ technique of K–Ar dating: a comparison with the conventional technique. Earth Planet. Sci. Lett. 12, 300–308.

Duan, C., Mao, J.W., Li, Y.H., Hou, K.J., Yuan, S.D., Zhang, C., Liu, J.L., 2011. Zircon U–Pb geochronology of the gabbro–diorite porphyry and granodiorite porphyry from Washan iron deposit in Ningwu basin, and its geological significance. Acta Geol. Sin. 85, 1159–1171 (in Chinese with English abstract).

Gao, L.K., Zou, Z.H., Li, S.C., Cai, W.D., Sun, X.H., Qian, L.Y., Zhang, L.S., 2015. Geological characteristics of the hydrothermal vein type gold–copper deposits in the Ningwu basin: a case study of the Tongiing Gold–Copper Deposit in Jiangsu Province. Geology and Resources 24, 117–123 (in Chinese with English abstract).

Hemley, J.J., Cygan, G.L., Fein, J.B., Robinson, G.R., d'Angelo, W.M., 1992. Hydrothermal ore-forming processes in the light of studies in rock-buffered system: I. Iron–copper–zinc–lead sulphide solubility reactions. Econ. Geol. 87, 1–22.

Hoskin, P.W.O., Black, L.P., 2000. Metamorphic zircon formation by solid-state recrystallization of protolith igneous zircon. J. Metamorph. Geol. 18, 423–439.

Hou, K.J., Yuan, S.D., 2010. LA–ICP–MS zircon U–Pb dating and Hf component of the magmatic rocks in Ningwu Cretaceous volcanic basin in Anhui Province and its geological significance. Acta Petrol. Sin. 26, 888–902 (in Chinese with English abstract).

Hou, K.J., Li, Y.H., Tian, Y.R., 2009a. In situ U–Pb zircon dating using laser ablation-multi ion counting-ICP-MS. Mineral Deposits 28 (4), 481–492 (in Chinesewith English abstract).

Hou, T., Zhang, Z.C., Du, Y., Li, S., 2009b. Geology of the Gushan iron oxide deposit associated with dioritic porphyries, eastern Yangtze craton, SE China. Int. Geol. Rev. 6, 520–541.

Hou, T., Zhang, Z.C., Encarnacion, J., Du, Y.S., Zhao, Z.D., Liu, J.L., 2010. Geochemistry of Late Mesozoic dioritic porphyries associated with Kiruna-style and stratabound carbonate-hosted Zhonggu iron ores, Middle-Lower Yangtze Valley, Eastern China: constraints on petrogenesis and iron sources. Lithos 119, 330–344.

Hou, T., Zhang, Z.C., Kusky, T., 2011. Gushan magnetite-apatite deposit in the Ningwu volcanic basin, Lower Yangtze River Valley, SE China: hydrothermal or Kiruna-type? Ore Geol. Rev. 43, 333–346.

Hou, T., Zhang, Z.C., Encarnacion, J., Huang, H., Wang, M., 2012. Geochronology/geochemistry of the Washan dioritic porphyry associated with Kiruna-type iron ores, Middle-Lower Yangtze River Valley, eastern China: implications for petrogenesis/mineralization. Int. Geol. Rev. 54, 1332–1352.

Hu, J.P., Jiang, S.Y., 2010. Zircon U–Pb dating and Hf isotopic compositions of Porphyrites from the Ningwu basin and their geological implications. Geol. J. China Univ. 16, 294–308 (in Chinese with English abstract).

Institute of Geochemistry, Chinese Academy of Sciences, 1987. Ore-forming Mechanism of Ninwu-type Iron Deposits. Science Press, Beijing, pp. 1–152 (in Chinese).

Jackson, S.E., Pearson, N.J., Griffin, W.L., Belousova, E.A., 2004. The application of laser ablation-inductively coupled plasma-mass spectrometry (LA-ICP-MS) to in situ U–Pb zircon geochronology. Chem. Geol. 211, 47–69.

Jensen, E.P., Barton, M.D., 2000. Gold deposits related to alkaline magmatism. Rev. Econ. Geol. 13, 279–314.

Jiangsu Geological Survey, 2010. Inventory Survey Report for Utilization of Resources and Reserves in the Checking Areas of the Tongjing Cu–Au Deposit in Nanjing City, Jiangsu Province. Internal Data. pp. 1–95 (in Chinese).

Layne, G.D., Spooner, E.T.C., 1991. The JC tin skarn deposit, southern Yukon Territory: I. Geology, paragenesis, and fluid inclusion microthermometry. Econ. Geol. 86, 29–47.

Li, B.L., Xie, Y.H., 1984. Origin, classification, and ore-forming model of Ninwu type iron deposits in the Ningwu area. Chin. Sci. (Ser. B) 1, 80–86 (in Chinese).

Li, J.W., Zhao, X.F., Zhou, M.F., Vasconcelos, P., Ma, C.Q., Deng, X.D., Zhao, Y.X., Wu, G., 2008. Origin of the Tongshankou porphyry–skarn Cu–Mo deposit, eastern Yangtze craton, Eastern China: geochronological, geochemical, and Sr–Nd–Hf isotopic constraints. Mineral. Deposita 43, 319–336.

Lin, X.D., 1999. Magmatic-Hydrothermal Transitional Type Deposit. China University of Geosciences Press, Wuhan, pp. 33–78 (in Chinese).

Liu, Y.S., Gao, S., Hu, Z.C., Gao, C.G., Zong, K.Q., Wang, D.B., 2010. Continental and oceanic crust recycling-induced melt–peridotite interactions in the Trans-North China Orogen: U–Pb dating, Hf isotopes and trace elements in zircons from mantle xenoliths. J. Petrol. 51, 537–571.

Lu, B., Hu, S.X., Lin, Y.S., Ye, S.Q., 1990. A study on origin and ore-forming model of Ninwu-type iron deposits. Mineral Deposits 9, 13–24 (in Chinese with English abstract).

Ludwig, K.R., 1999. Using Isoplot/Ex, version 2.01, a geochronogical toolkit for Microsoft Excel. Berkeley Geochronology Center Special Publication 1a, p. 47.

Ludwig, K.R., 2003. User's manual for Isoplot 3.00: a geochronological toolkit for Microsoft Excel. Berkeley Geochronology Center Special Publication 4.

Mao, J.W., Wang, Y.T., Lehmann, B., Yu, J.J., Du, A.D., Mei, Y.X., Li, Y.F., Zang, W.S., Stein, H.J., Zhou, T.F., 2006. Molybdenite Re–Os and albite $^{40}Ar/^{39}Ar$ dating of Cu–Au–Mo and magnetite porphyry systems in the Yangtze River valley and metallogenic implications. Ore Geol. Rev. 29, 307–324.

Mao, J., Xie, G., Duan, C., Pirajno, F., Ishiyama, D., Chen, Y., 2011. A tectono-genetic model for porphyry–skarn–stratabound Cu–Au–Mo–Fe and magnetite–apatite deposits along the Middle-Lower Yangtze River Valley, Eastern China. Ore Geol. Rev. 43, 294–314.

Mao, J.W., Duan, C., Liu, J.L., Zhang, C., 2012. Metallogeny and corresponding mineral deposit model of the Cretaceous terrestrial volcanic-intrusive rock-related polymetallic iron deposits in Middle-Lower Yangtze River Valley. Acta Petrol. Sin. 28, 1–14 (in Chinese with English Abstract).

McDougall, I., Harrison, T.M., 1999. Geochronology and Thermochronology by the $^{40}Ar/^{39}Ar$ Method. Oxford University Press, Oxford.

Muecke, G.K., Elias, P., Reynolds, P.H., 1988. Hercynian/Alleghanian overprinting of an acadian terrane: $^{40}Ar/^{39}Ar$ studies in the Meguma zone, Nova Scotia, Canada. Chem. Geol. 73, 153–167.

Ningwu Research Group, 1978. Ningwu Porphyrite Iron Ores. Geological Publishing House, Beijing, pp. 1–196 (in Chinese).

Pan, Y., Dong, P., 1999. The Lower Changjiang (Yangzi/Yangtze River) metallogenic belt, east central China: intrusion- and wall rock-hosted Cu–Fe–Au, Mo, Zn, Pb, Ag deposits. Ore Geol. Rev. 15, 177–242.

Peng, J.T., Zhou, M.F., Hu, R.Z., Shen, N.P., Yuan, S.D., Bi, X.W., Du, A.D., Qu, W.J., 2006. Precise molybdenite Re–Os and mica Ar–Ar dating of the Mesozoic Yaogangxian tungsten deposit, central Nanling district, South China. Mineral. Deposita 41, 661–669.

Sheppard, S.M.F., 1986. Characterization and isotopic variations in natural waters. Rev. Mineral. 16, 165–183.

Sláma, J., Kosler, J., Condon, D.J., Crowley, J.L., Gerdes, A., Hanchar, J.M., Horstwood, M.S.A., Morris, G.A., Nasdala, L., Norberg, N., Schaltegger, U., Schoene, B., Tubrett, M.N., Whitehouse, M.J., 2008. Plesovice zircon — a new natural reference material for U–Pb and Hf isotopic microanalysis. Chem. Geol. 249, 1–35.

Steiger, R.H., Jager, E., 1977. Subcommission on geochronology: convention on the use of decay constants in geo- and cosmochronology. Earth Planet. Sci. Lett. 36, 359–362.

Tang, Y.C., Wu, Y.C., Chu, G.Z., Xing, F.M., Wang, Y.M., Cao, F.Y., Chang, Y.F., 1998. Geology of Copper-Gold Polymetallic Deposits Along the Changjiang Area of Anhui Province. Geological Publishing House, Beijing, pp. 1–351 (in Chinese with English abstract).

Urabe, T., 1985. Aluminum granite as source magma of hydrothermal ore deposits: an experimental study. Econ. Geol. 80, 148–157.

Wang, S.S., 1983. Dating of the Chinese K–Ar standard sample (Fangshan biotite, ZBH-25) by using the $^{40}Ar/^{39}Ar$ method. Sci. Geol. Sin. 4, 315–321 (in Chinese with English abstract).

Wang, Y.F., 2009. A Study on Volcanic Rocks of the Niangniangshan Formation in the Ningwu Basin (Master Degree Dissertation) China University of Geosciences, Beijing, pp. 1–108 (in Chinese with English abstract).

Wang, D.Z., Ren, Q.J., Qiu, J.S., Chen, K.R., Xu, Z.W., Zeng, J.H., 1996. Characteristics of volcanic rocks in the shoshonite province, Eastern China and their metallogenesis. Acta Geol. Sin. 70, 23–34 (in Chinese with English abstract).

Wang, Y.L., Zhang, Q., Wang, Y., 2001. Geochemical characteristic of the volcanic rocks in the Ningwu area and its significance. Acta Petrol. Sin. 565–575 (in Chinese with English abstract).

Wang, Q., Wyman, D.A., Xu, J.F., Zhao, Z.H., Jian, P., Xiong, X.L., Bao, Z.W., Li, C.F., Bai, Z.H., 2006. Petrogenesis of Cretaceous adakitic and shoshonitic igneous rocks in the Luzong area, Anhui Province (eastern China): implications for geodynamics and Cu–Au mineralization. Lithos 89 (3–4), 424–446.

Wu, F.Y., Lin, J.Q., Wilde, S.A., Zhang, X.O., Yang, J.H., 2005. Nature and significance of the Early Cretaceous giant igneous event in eastern China. Earth Planet. Sci. Lett. 233, 103–119.

Wyman, D.A., Kerrich, R., 1988. Alkaline magmatism, major structures, and gold deposits; implications for greenstone belt gold metallogeny. Econ. Geol. 83, 454–461.

Xie, G.Q., Mao, J.W., Zhao, H.J., Duan, C., Yao, L., 2012. Zircon U–Pb and phlogopite $^{40}Ar–^{39}Ar$ age of the Chengchao and Jinshandian skarn Fe deposits, southeast Hubei Province, Middle–Lower Yangtze River Valley metallogenic belt, China. Mineral. Deposita 47, 633–652.

Xu, Z., 1990. Mesozoic volcanism and volcanogenic iron-ore deposits in eastern China. Geol. Soc. Am. Spec. Pap. 237, 1–46.

Xu, W.G., Fan, H.R., Hu, F.F., Santosh, M., Yang, K.F., Lan, T.G., Wen, B.J., 2014. Gold mineralization in the Guilaizhuang deposit, southwestern Shandong Province, China: insights from phase relations among sulfides, tellurides, selenides and oxides. Ore Geol. Rev. 56, 276–291.

Xue, H.M., Dong, S.W., Ma, F., 2010. Zircon U–Pb SHRIMP ages of subvolcanic bodies related to porphyry Fe-deposits in the Luzong and Ningwu basins, Middle and Lower Yangtze River Reaches, Central China. Acta Petrol. Sin. 26, 2653–2664 (in Chinese with English abstract).

Yan, J., Liu, H.Q., Song, C.Z., Xu, X.S., An, Y.J., Liu, J., Dai, L.Q., 2009a. Zircon U–Pb geochronology of the volcanic rocks from Fanchang–Ningwu volcanic basins in the Lower Yangtze region and its geological implications. Chin. Sci. Bull. 54, 2895–2904.

Yan, J., Yu, Y.F., Chen, J.F., 2009b. Rb–Sr isotopic dating of volcanic rocks from the Niangniangshan Formation in the Nanjing–Wuhu area and its geological implications. Geogr. Rev. 55, 121–125 (in Chinese with English abstract).

Yu, J.J., Mao, J.W., 2004. $^{40}Ar–^{39}Ar$ dating of albite and phlogopite from porphyry iron deposit in the Ningwu basin in east-central China and its significance. Acta Geol. Sin. 78, 435–442.

Yu, J.J., Chen, Y.C., Mao, J.W., Pirajno, F., Duan, C., 2011. Review of geology, alteration and origin of iron oxide–apatite deposits in the Cretaceous Ningwu volcanic basin, Lower Yangtze River Valley, eastern China: implications for ore genesis and geodynamic setting. Ore Geol. Rev. 43, 170–181.

Yu, J.J., Che, L.R., Wang, T.Z., 2015a. Geology, alteration, oxygen isotope and fluid inclusion study of the Meishan iron oxide–apatite deposit, southeast China. Mineral. Deposita 50, 847–869.

Yu, J.J., Lu, B.C., Wang, T.Z., Che, L.R., 2015b. Cretaceous Cu–Au, pyrite, and Fe-oxide–apatite deposits in the Ningwu basin, Lower Yangtze Area, Eastern China. J. Asian Earth Sci. 103, 150–168.

Yuan, S.D., Hou, K.J., Liu, M., 2010. Timing of mineralization and geodynamic framework of iron–oxide–apatite deposits in the Ningwu Cretaceous volcanic basin in the Middle and Lower reaches of the Yangtze River, China: constraints from Ar–Ar dating on phlogopites. Acta Petrol. Sin. 26, 797–808 (in Chinese with English Abstract).

Yuan, F., Zhou, T.F., Fan, Y., Zhang, L.J., Ma, L., Qian, B., 2011. Zircon U–Pb ages and isotopic characteristics of the granitoids in the Ningwu basin, China. Acta Geol. Sin. 85, 821–833 (in Chinese with English abstract).

Zhai, Y.S., Yao, S.Z., Lin, X.D., Zhou, X.R., Wan, T.F., Jin, F.J., Zhou, Z.G., 1992. Fe–Cu (Au) Metallogeny of the Middle-Lower Changjiang Region. Geological Publishing House, Beijing, pp. 1–235 (in Chinese).

Zhang, R.H., 1979. Geochemical zoning of the altered country rock of the porphyry iron ore in the middle-lower Changjiang Valley. Acta Geol. Sin. 53, 137–152 (in Chinese with English abstract).

Zhang, Q., Jian, P., Liu, D.Y., 2003. SHRIMP dating of volcanic rocks from Ning-Wu areas and its geological implications. Sci. China Ser. D Earth Sci. 33, 309–314 (in Chinese).

Zhang, Y.M., Gu, X.X., Liu, L., Dong, S.Y., Li, K., Li, B.H., Lü, P.R., 2011. Fluid inclusion and H–O isotope evidence for immiscibility during mineralization of the Yinan Au–Cu–Fe deposit, Shandong, China. J. Asian Earth Sci. 42, 83–96.

Zhou, T.F., Yuan, F., Yue, S.C., Liu, X.D., Zhang, X., Fan, Y., 2007. Geochemistry and evolution of ore-forming fluids of the Yueshan Cu–Au skarn- and vein-type deposits, Anhui Province, South China. Ore Geol. Rev. 31, 279–303.

Zhou, T.F., Fan, Y., Yuan, F., Zhang, L.J., Qian, B., Ma, L., Yang, X.F., Cooke, D.R., 2011. Geochronology and significance of volcanic rocks in the Ning-Wu Basin of China. Sci. China Earth Sci. 54, 185–196.

Zhou, T., Fan, Y., Yuan, F., Zhang, L.J., Qian, B., Ma, L., Yang, X.F., 2013. Geology and geochronology of magnetite–apatite deposits in the Ning-Wu volcanic basin, Eastern China. J. Asian Earth Sci. 66, 90–107.